J Fluoresc (2011) 21:299–312
DOI 10.1007/s10895-010-0717-y

ORIGINAL PAPER

Simultaneous pH and Temperature Measurements Using Pyranine as a Molecular Probe

Felix H. C. Wong · Cécile Fradin

Received: 5 April 2010 / Accepted: 8 September 2010 / Published online: 5 October 2010

Abstract Steep variations in concentration and temperature frequently occur in small fluid compartments such as those found in cells or microfluidic devices. A quantitative characterization of concentration and temperature gradients is therefore required before these systems can be fully understood. Although different spatially resolved fluorescence methods have been developed to measure either the temperature or the concentration of ions such as proton or calcium, often concentration measurements depend on temperature and vice versa. Here, we describe a method allowing simultaneous measurement of pH and temperature. This method is based on the detection of the blinking of the fluorescent pH indicator pyranine, a process due to its alternating between a basic form and an acidic form. Fluorescence correlation spectroscopy allows measuring both the protonation and deprotonation rates of pyranine, and each pair of rates can be uniquely related to a pair of pH and temperature values. We show, however, that the relationship between rates, pH and temperature, is very sensitive to the presence of other acid-base molecules in solution. We also show that it is influenced by the overall ionic strength of the solution, in a manner that depends on buffer composition.

Keywords Fluorescence · Fluorescence correlation spectroscopy · Protonation · Photophysics · Ionic strength · Pyranine

F. H. C. Wong · C. Fradin
Department of Physics and Astronomy, McMaster University, Hamilton, ON, Canada

C. Fradin (✉)
1280 Main St W,
Hamilton, ON L8S4M1, Canada
e-mail: fradin@physics.mcmaster.ca

Introduction

Picoliter compartments such as those found in microfluidic devices and in living cells can harbor significant variations in molecular concentrations and in temperature over distances as short as a few micrometers. In microfluidic devices, sharp gradients can be created and controlled by combining several fluid flows into a single narrow channel [1, 2], and they may also unexpectedly arise from differences between the properties of the fluid and that of the chamber, for example from a temperature mismatch [3, 4]. In cells, many cellular events can lead to local changes in either molecular concentration (including pH) or temperature. Intracellular signaling and the establishment of cell polarity, for example, are both based on the creation of sharp molecular gradients across the cell [5, 6]. Proton gradients build up across the inner and outer mitochondrial membrane as a result of ATP synthesis [7], and across the membrane of liposomes during endocytosis [8–10]. ATP hydrolysis can result in localized heat production at the mitochondria or the endoplasmic reticulum [11, 12]. Spatially resolved methods allowing quantitative concentration or temperature measurements are therefore important tools for the study of the underlying processes leading to gradient formations in these systems.

Of all possible methods for pH and temperature measurements, optical methods allow submicron spatial resolutions and have the advantage of being non-invasive. Among these, fluorescence methods present the additional advantage of being highly sensitive. The simplest fluorescence methods rely on the measurement of pH or temperature dependent fluorescence emission intensity of a fluorescent probe. For example, the fluorescence quantum yield of BCECF is highly sensitive to pH, and therefore the fluorescence intensity of a solution containing a small

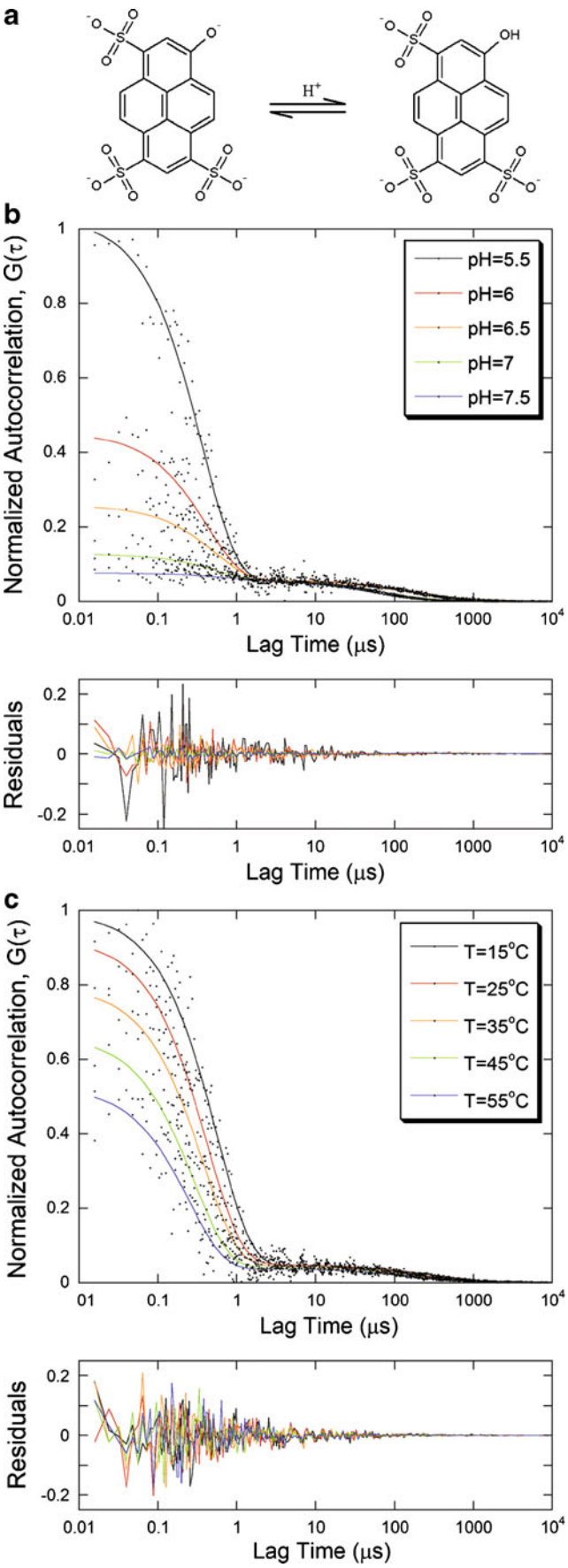

Fig. 1 Pyranine photophysics due to reversible protonation as observed by FCS. **a** Molecular structures of the protonated and deprotonated forms of pyranine. **b** Autocorrelation functions obtained from pyranine in PBS at various pHs (T=30 °C). **c** Autocorrelation functions of pyranine in PBS (pH=5.5) for different temperatures. Data were fitted with Eq. 1 and normalized to obtain the same amplitude of the diffusion term. The residuals of the fits are shown in the lower panels

concentration of this dye can be used as an indication of pH [13]. Similarly, the fluorescence quantum yield of rhodamine B changes with temperature, allowing temperature measurements [14]. These methods, however, are not appropriate for characterizing spatial gradients if either the excitation intensity, the collection efficiency or the concentration of the fluorescent probe is not uniform across the field of view. A more refined approach is therefore to use ratiometric methods, where two different fluorescence quantities are measured and compared through the calculation of their ratio, which eliminates any dependence on instrument characteristics or probe concentration [15]. This method has been widely applied for in vivo pH measurements, using the ratio of the emission intensities collected at two different wavelengths [8, 9, 16, 17]. Another possible approach is to measure a quantity that is not dependent on concentration, such as the probe diffusion coefficient [18], its fluorescence lifetime [2, 19], or the relaxation time of the fluorescence blinking generated from association and dissociation of protons to the fluorescent probe [20, 21].

In that context, we recently proposed to use the relaxation time associated with EGFP blinking for temperature measurements [22]. In the presence of protons, EGFP constantly switches between a deprotonated form which is fluorescent under 488 nm excitation, and a protonated form which is not, causing a blinking which can be quantified using fluorescence correlation spectroscopy (FCS) [23]. We showed that the relaxation time associated with this blinking is strongly temperature-dependent and that it can therefore be used as a gauge to measure temperature [22]. However, the equally strong dependence of this parameter on other variables, in particular pH and buffer concentration [20, 23], requires attention. In addition, detection of protonation-dependent blinking by FCS is most sensitive at or below the probe pK_a, that is below pH~6 for EGFP [22]. Finally, although GFP derivatives are expected to be useful in a cellular context since they can be genetically encoded, the use of organic fluorophores allows more flexibility in general.

Here we report on our investigations of the well-known pH sensitive dye 8-Hydroxypyrene-1,3,6-trisulfonic acid trisodium salt (pyranine or HPTS) as a possible combined pH and temperature indicator. Pyranine is a small, negatively charged organic fluorophore which is soluble in water and membrane

impermeable [24]. Pyranine possesses a hydroxyl group and, like EGFP, it can exist in a protonated and a deprotonated form (Fig. 1a). Both are fluorescent, but with very different excitation maxima: 405 nm for protonated pyranine, and 450 nm for deprotonated pyranine [24, 25]. Pyranine is therefore an excellent probe for ratiometric pH measurements. It has been used to measure pH in very different contexts, for example inside and on the outer surface of liposomes [25], in endocytic vesicles [8] and in endocytic organelles in neurons [9]. In addition, pyranine has been often used as a photoacid to study proton transfer in acid-base reactions [26–32]. Since pyranine has a pK_a~7.2, we postulated that it would exhibit a detectable fluorescence blinking around physiological pH and below. We were able to detect this blinking using FCS under 442 nm excitation. Since the fraction of non-fluorescent molecules and the relaxation rate associated with blinking, which are both accessible by FCS, are strongly pH- and temperature-dependent, we propose that detection of pyranine blinking by FCS can be used to measure pH and temperature simultaneously. We investigated the influence of buffer and salt concentration on the protonation reaction, in order to establish the robustness of these measurements.

Materials and Methods

Sample Preparation

For FCS measurements, stock solutions of pyranine (Sigma-Aldrich) were diluted in a buffer solution, down to concentrations that ranged from 40 nM to 750 nM, depending on the pH of the solvent. Different types of buffer were used: Standard PBS (10 mM Na_2HPO_4, 2 mM KH_2PO_4, 137 mM NaCl, 2.7 mM KCl), modified PBS (where the concentration of one component was modified compared to standard PBS), basic phosphate buffer (10 mM Na_2HPO_4, 2 mM KH_2PO_4, and various concentrations of NaCl or KCl), and HEPES buffers (20 mM HEPES, and various concentrations of NaCl, KCl, $MgCl_2$, or $CaCl_2$). Due to the formation of magnesium and calcium phosphate precipitates, $MgCl_2$ and $CaCl_2$ ions were not used in phosphate buffers. All buffers were prepared with double distilled water. The pH of the buffers was adjusted by addition of HCl or NaOH, and measured using a digital pH meter. The ionic strength of the buffers was calculated according to:

$$\mu = \frac{1}{2}\sum_i c_i z_i^{\,2}$$

where c_i and z_i are the concentration and charge of ion i, respectively. It was considered that HEPES, a zwitterion, did not contribute to the ionic strength as suggested by Stellwagen *et al.* [33].

Fluorescence Correlation Spectroscopy

FCS experiments were performed on a home-built FCS instrument [34]. The 442 nm line of a He-Cd laser (Liconix, Santa Clara, CA) was first directed through a variable neutral density filter (Thorlabs, Newton, NJ) for adjustment of the laser beam power, which was measured using an optical power meter (Newport, Irvine, CA). It next passed through an adjustable iris allowing changing the beam diameter, in order to vary the size of the confocal detection volume. The beam then entered the back port of an inverted microscope (Nikon Eclipse TE2000-U, Nikon, Tokyo, Japan), where it passed through a band pass excitation filter (D436/10x, Chroma, Rockingham, VT) before being reflected upward by a dichroic mirror (455DCLP, Chroma, Rockingham, VT), into the back aperture of an air immersion objective (Plan Apo 60x 0.95NA, Nikon, Tokyo, Japan). Emitted fluorescence was collected by the same objective, passed through the dichroic mirror and through an emission filter (E475LPv2, Chroma, Rockingham, VT), and was focused through a pinhole in order to remove out-of-focus fluorescence. Five different sizes of pinhole were used, 50-, 75-, 100-, 150-, and 200-μm (purchased from Thorlabs), depending on the diameter of the excitation laser beam. Finally, the emitted fluorescence was separated by a 50/50 beam splitter (Chroma, Rockingham, VT) into two separate channels, and detected by two photomultiplier tubes (H7421, Hamamatsu Photonics, Hamamatsu City, Japan). The collected signals were fed to a multiple-tau correlator (Flex02-08D, Correlator.com, Bridgewater, NJ) that performed correlation analysis. Pinhole alignment and data acquisition were handled by a program written for Labview (National Instruments, Austin, TX). Most samples were placed in a chamber made by a microscope slide and a cover slip spaced by parafilm and sealed with wax. The temperature of such samples was controlled using an inverted microscope stage temperature control system (PE-100NI, Linkam Scientific, Surrey, UK). For microfluidic measurements, chips made of PDMS (microfluidic ChipShop, Jena, Germany) were used. The cross section of the microfluidic channel was a trapezoid, with a height of 20 μm, and a width varying between 92 μm and 120 μm. The inlet of the microfluidic chip was connected to a 20 ml syringe through a silicon tube. The syringe was then loaded on a digital infusion syringe pump (SP100i, World Precision Instruments, Inc.), dispensing flow rates between 0.03 and 1 ml/hour. For all samples, at least 5 individual FCS measurements were performed, each lasting between 30 and 200 s.

Analysis of the Autocorrelation Functions

In the absence of flow, autocorrelation functions were analyzed assuming pyranine was freely diffusing and undergoing a blinking process with exponentially distributed dwell times [23]:

$$G(\tau) = \frac{1}{N}\left(1+\frac{\tau}{\tau_D}\right)^{-1}\left(1+\frac{\tau}{S^2\tau_D}\right)^{-\frac{1}{2}}\left[1+\frac{B}{1-B}\exp\left(\frac{-\tau}{\tau_B}\right)\right] \quad (1)$$

S is the aspect ratio of the ellipsoidal confocal volume. N is the average number of pyranine molecules present in the confocal volume, and τ_D is indicative of their residence time in that volume. τ_B is the relaxation time associated with pyranine blinking, and B is the average fraction of pyranine molecules found in the dark state.

At the beginning of each series of measurements, fluorescein was used to determine the half-width, w_0, and half-height, z_0, of the confocal detection volume. Fluorescein has a known diffusion coefficient, D=410 μm^2/s at 20 °C [35], which allows calculating w_0 using the expression: $\tau_D = {w_0}^2/4D$, while z_0 can be calculated using the aspect ratio: $S = z_0/w_0$. The effective confocal volume is given by: $V = \pi^{3/2}{w_0}^2 z_0$, and allows estimating fluorophore concentrations: $c = N/V$.

In the presence of flow the expression of the autocorrelation function requires an additional term [36, 37]:

$$G(\tau)_{flow} = G(\tau)\cdot\exp\left[-\left(\frac{\tau}{\tau_{flow}}\right)^2\left(1+\frac{\tau}{\tau_D}\right)^{-1}\right] \quad (2)$$

where τ_{flow} is related to the flow rate, $v = w_0 / \tau_{flow}$.

In all cases, we used the software KaleidaGraph (Synergy Software, Reading, PA) to analyze the obtained autocorrelation functions. Each reported parameter value represents an average value for at least five individual measurements, and the associated error corresponds to either the average error returned by the fitting program or the standard deviation of the five individual parameter values, whichever was the largest.

Determination of the Reaction Rates Associated with Protonation and Deprotonation

Assuming that the fraction of non-fluorescent pyranine molecules, B, corresponds to the fraction of protonated pyranine molecules, we have:

$$B = \frac{[AH]}{[AH]+[A^-]}$$

where [AH] is the concentration of protonated pyranine and [A$^-$] is the concentration of deprotonated pyranine. We can therefore relate B to the equilibrium constant associated with the protonation reaction, K, using the Henderson-Hasselbalch equation:

$$K = \frac{[HA]}{[H^+][A^-]} = \frac{1}{10^{-pH}}\cdot\frac{B}{1-B}.$$

B is therefore expected to vary with pH according to:

$$B = \left(10^{pH-pK_a}+1\right)^{-1} \quad (3)$$

where $pK_a = \log K$ is not expected to vary significantly with pH.

The rate constants for protonation, k_p, and for deprotonation, k_d, can be calculated from the experimentally accessible parameters B and τ_B, since $K = k_p / k_d$ and since:

$$\tau_B = \frac{1}{[H^+]\cdot k_p + k_d}. \quad (4)$$

Therefore:

$$k_p = \frac{B}{\tau_B\cdot 10^{-pH}} \quad (5)$$

and

$$k_d = \frac{1-B}{\tau_B}. \quad (6)$$

Temperature Dependence of the Thermodynamic Parameters Associated with Protonation and Deprotonation

For a blinking process due to a reversible chemical reaction with rate constants obeying Arrhenius' law, the two experimentally accessible quantities associated with the blinking, τ_B and K, should depend on temperature according to:

$$\tau_B = \left[10^{-pH}\cdot A_p\exp\left(-\frac{E_p}{RT}\right)+A_d\exp\left(-\frac{E_d}{RT}\right)\right]^{-1} \quad (7)$$

and:

$$\ln(K) = -\frac{\Delta E}{RT}+\ln\left(\frac{A_p}{A_d}\right), \quad (8)$$

where R is the gas constant. E_p and E_d are the activation energies for protonation and deprotonation respectively, and $\Delta E = E_p - E_d$. A_p and A_d are the frequency factors for protonation and deprotonation, respectively.

Another way to relate K to temperature is to use the relationship between the free energy change associated with the reaction, ΔG, and the equilibrium constant, K:

$$\Delta G = -RT\ln K$$

and to combine this relationship with the Gibbs free energy equation:

$$\Delta G = \Delta H - T\Delta S.$$

Assuming that the enthalpy change, ΔG, and entropy change, ΔS, associated with protonation do not significantly depend on temperature, the temperature dependence of the pK_a should be:

$$pK_a = -\frac{1}{2.303R} \cdot \left(\frac{\Delta H}{T} - \Delta S\right). \quad (9)$$

Results

Pyranine Protonation Observed with Fluorescence Correlation Spectroscopy

We used FCS to study solutions of pyranine in phosphate buffer (standard PBS) for pHs ranging between 4 and 9 and for temperatures ranging from 15 °C to 55 °C. We used a 442 nm excitation wavelength, at which only the non-protonated form of pyranine is fluorescent, so that reversible protonation of the fluorophore should result in detectable fluorescence fluctuations. As expected, the autocorrelation functions (ACFs) obtained showed two distinct decays, one around 100 μs characteristic of fluorophore diffusion, and one around 1 μs which we attributed to reversible fluorophore protonation (Fig. 1b & c). We consequently analyzed all ACFs using Eq. 1. Representative parameters extracted from this analysis and their associated errors are listed in Table 1. The residence time, τ_D, and the relaxation time associated with the blinking of pyranine, τ_B, obtained from the analysis of the ACFs recorded at 20 and 50 °C, are shown in Fig. 2a. The reduction in apparent residence time observed at high pH is probably due to photobleaching of pyranine in conditions where the probability for a pyranine molecule to be in its deprotonated fluorescent state is high. However, because the relaxation time is separated from the apparent residence time by more than two orders of magnitude, this should not affect measurement of τ_B. The average fraction of pyranine in the non-fluorescent state, B, is shown in Fig. 2b. In agreement with the hypothesis that this non-fluorescent state corresponds to the protonated state of the fluorophore, B switches from a value of ~1 at low pH to a value of ~0 at high pH according to the Henderson-Hasselbalch equation (Eq. 3, with the addition of a small background term). This analysis returns a value of the pK_a which slightly decreases with temperature, from ~7.1 at 15 °C to ~6.9 at 55 °C. This range of values is in good agreement with previously reported values for the pK_a of pyranine [24, 25, 38]. Assuming that the enthalpy change (ΔH) and entropy change (ΔS) associated with pyranine protonation are constant in the temperature range explored, the linear dependence of the pK_a on inverse temperature (Fig. 2c) can be understood in terms of Gibbs equation for the free energy of a reaction (Eq. 10). Doing so provides ΔH~-10± 1 kJ/mol and ΔS~0.101±0.003 kJ/(K.mol).

Temperature- and pH- Dependence of the Reversible Protonation of Pyranine

When considering the ACFs recorded at a given pH for different temperatures (Fig. 1c), we observed that both the amplitude of the photophysics term (related to the fraction of protonated pyranine) and its characteristic decay time (related to the relaxation time associated with pyranine protonation) decreased with increasing temperature. Analysis of these ACFs allowed obtaining the relaxation time associated with pyranine protonation and deprotonation as a function of temperature (Fig. 3a), as well as the natural log of the equilibrium constant of the reaction (shown in Fig. 3b as a function of the inverse of temperature). The relaxation time showed a stronger

Table 1 Parameters extracted from the fit of autocorrelation functions such as those shown in Fig. 1 using Eq. 1. The reported value is the mean of five individual measurements, and the reported error is the corresponding standard deviation (which in this case was always larger than the fitting error of each individual measurement)

	pH	τ_D (μs)	B	τ_B (μs)
T=30 °C	5.5	173±60	0.939±0.004	0.417±0.039
	6.0	189±39	0.874±0.008	0.441±0.037
	6.5	156±22	0.779±0.014	0.532±0.059
	7.0	67±4	0.536±0.012	0.655±0.097
	7.5	53±3	0.253±0.017	0.835±0.226
	T (°C)	τ_D (μs)	B	τ_B (μs)
pH=5.5	15	230±107	0.946±0.005	0.551±0.040
	25	199±79	0.942±0.004	0.459±0.030
	35	143±39	0.935±0.004	0.366±0.021
	45	135±47	0.927±0.005	0.329±0.028
	55	107±35	0.914±0.007	0.283±0.018

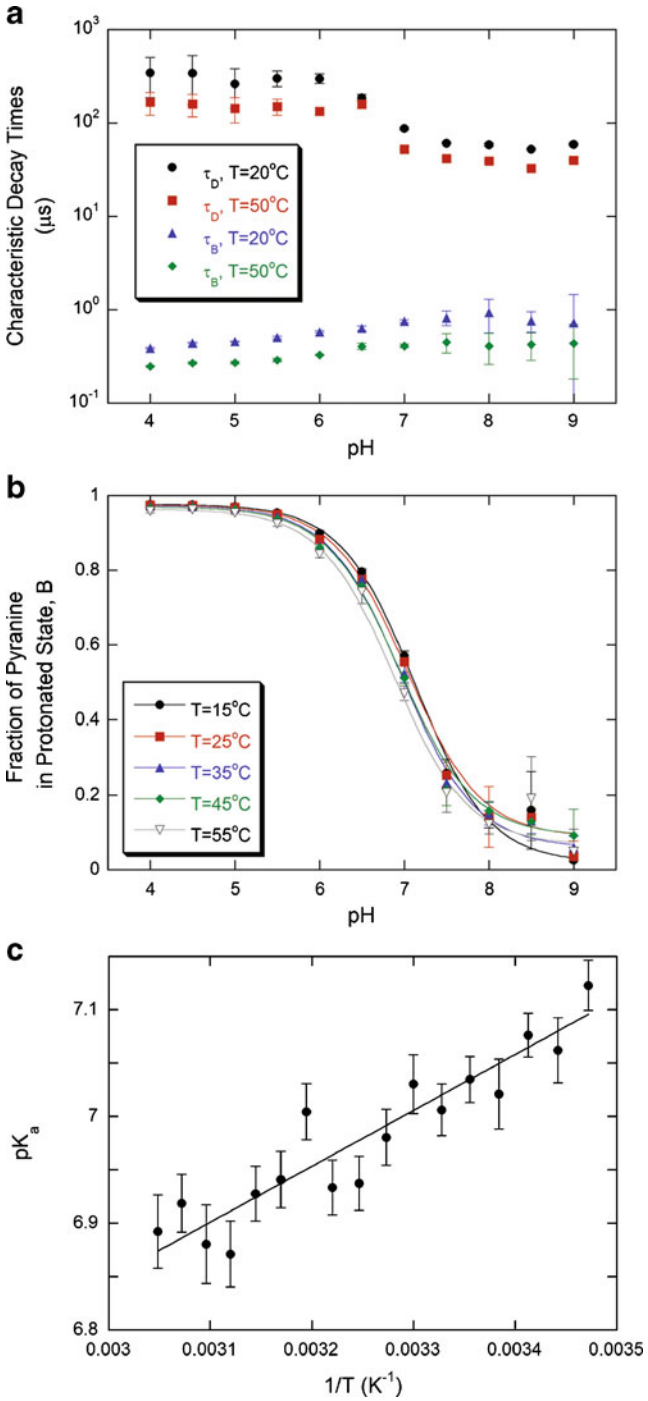

Fig. 2 **a** Average residence time and relaxation time measured for pyranine as a function of pH in the detection volume. **b** Fraction of pyranine in protonated state as a function of pH at various temperatures. Data were fitted with Eq. 3. **c** Dissociation constant of pyranine as a function of the inverse absolute temperature. Data were fitted with Eq. 9

temperature dependence for pHs approaching the pK_a of pyranine, however the error on the measured values of the relaxation time also became larger with increasing pH. Assuming that the rate constant for protonation and deprotonation are following Arrhenius' law, the temperature dependence of the equilibrium constant and relaxation time associated with the protonation reaction should be accurately captured by Eqs. 7 and 8. We found that this was the case, and fitting of the data with these equations provided the values of the frequency factors (Fig. 4a) and of the activation energies (Fig. 4b) of the protonation/deprotonation process at each of the different pHs studied.

Possibility of Combined pH and Temperature Measurements Using Pyranine

The fraction of protonated pyranine, B, depends strongly on pH and weakly on temperature, while the protonation

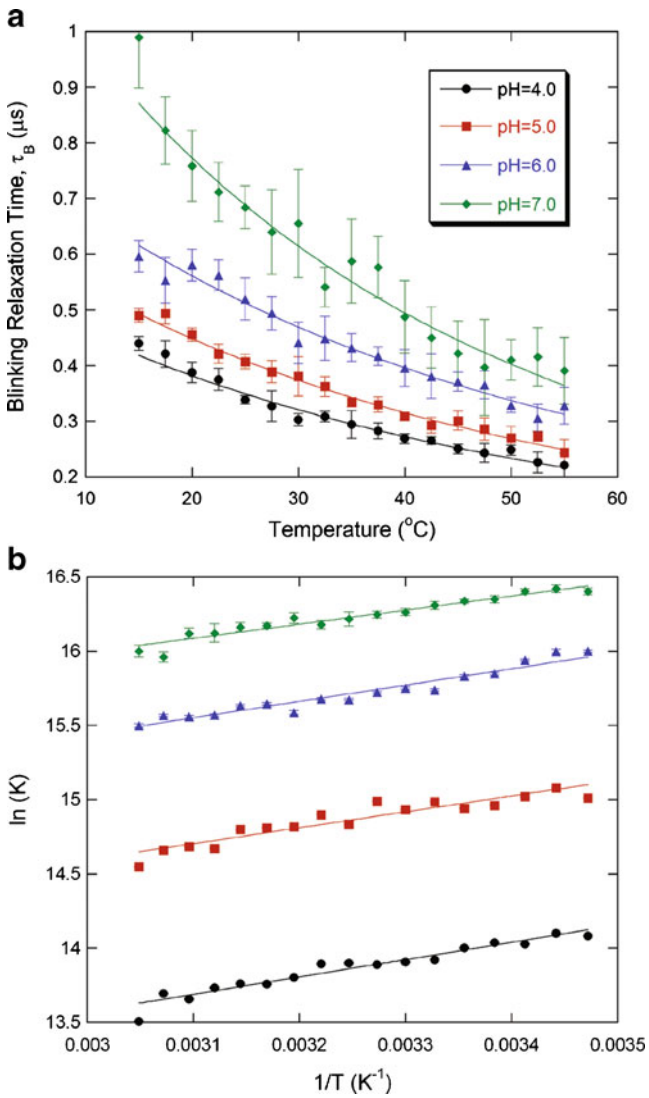

Fig. 3 **a** Blinking relaxation time of pyranine against temperature at different pHs. Data were fitted with Eq. 8. Errors correspond to standard deviations obtained from multiple measurements. **b** Equilibrium constant of the protonation / deprotonation reaction determined from pyranine's blinking as a function of the inverse absolute temperature at various pH. Data were fitted with Eq. 7

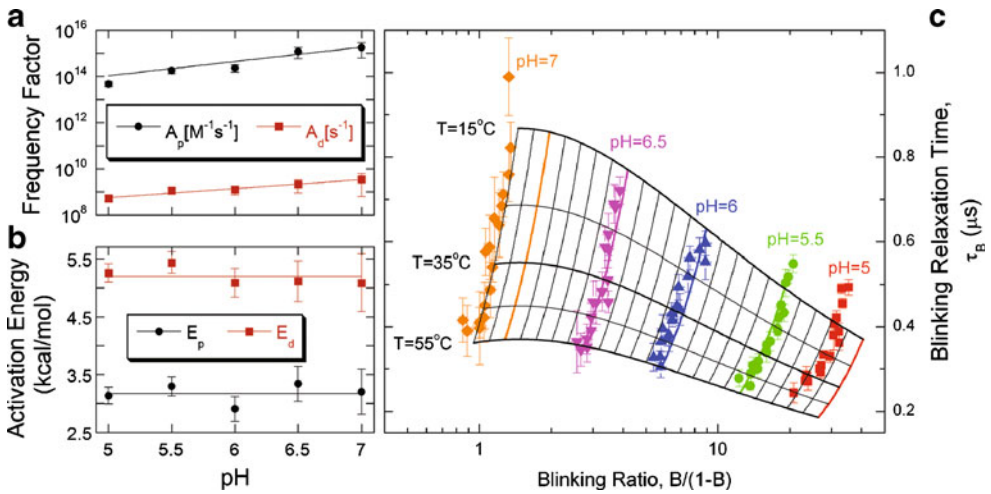

Fig. 4 **a** Frequency factors and **b** activation energies associated with the protonation and deprotonation rates of pyranine at various pHs. **c** Blinking relaxation time against blinking ratio corresponding to the reversible protonation of pyranine. The solid lines represent the expected dependence at either fixed pH or fixed temperature. The same color is used for the data at a given pH and the corresponding expected dependence at that pH. The following empirical expressions were obtained from the data shown in (**a**) and (**b**) for the dependence of the frequency factors and activation energies on pH: E_p=3.2*kcal.mol*$^{-1}$; E_d=5.2*kcal.mol*$^{-1}$; $A_p=8.8\times10^{10}\cdot(1.4\cdot pH)\ M^{-1}.s^{-1}$; $A_d=6.3\times10^{6}\cdot\exp(0.9\cdot pH)s^{-1}$. These expressions were used to calculate the expected dependence shown in (**c**)

relaxation time, τ_B, depends strongly on temperature and weakly on pH (Fig. 4c). This makes measuring temperature and pH using these parameters independently difficult. On the other hand, each combination of values for B and τ_B corresponds to a unique combination of pH and temperature. Therefore, by measuring both B and τ_B (as done with FCS), one should be able to determine accurately both pH and temperature. In order to relate B and τ_B to pH and temperature, we first found two empirical expressions to calculate the frequency factors and the activation energies for protonation and deprotonation as a function of pH (Fig. 4a and b, with empirical expressions in the figure caption). It was then possible to determine the iso-temperature and iso-pH lines using these expressions. Such lines are plotted in Fig. 4c, showing that around pH~6 and T~30 °C, both these parameters can be determined from B and τ_B with a precision of ~0.1 pH unit and ~2 °C, using the empirical expressions mentioned above and an inverted form of Eqs. 7 and 8. The measurement range can be extended by using an experimental calibration method (i.e. the data points in Fig. 4c) rather than inverted equations (i.e. the lines in Fig. 4c).

Sensitivity of the Measurement to Excitation Intensity, Size of the Detection Volume, Pyranine Concentration and Liquid Flow

One advantage of the pH and temperature measurement proposed above is that the values of the blinking parameters measured by FCS should not depend on experimental implementation (such as excitation intensity or exact size of the confocal detection volume) or pyranine concentration. We therefore investigated whether the excitation power, the concentration of pyranine, and the size of the confocal detection volume had any influence on the values measured for B and τ_B by FCS (for pyranine in PBS). We used a range of values for these parameters (excitation intensities from 30 to 500 μW, pyranine concentrations from 30 to 300 nM, and radii of the confocal observation volume from 0.4 to 1.7 μm) that included the range usually used for FCS experiments. The results of these experiments are shown in Fig. 5. They indicated that, as expected, neither the measured fraction of protonated pyranine molecules, B, nor the measured blinking relaxation time, τ_B, was affected by the excitation intensity (at least below 300 μW), the size of the observation volume or the fluorophore concentration.

For pH and temperature measurement proposed to be applicable in systems such as microfluidic channels or living cells, the measurement should also be insensitive to the eventual presence of liquid flow. We therefore performed FCS experiments for pyranine solutions flowing in a microfluidic chip. ACFs recorded for different velocities of the laminar flow are shown in Fig. 6a. While the decay time corresponding to the residence time of the pyranine molecules in the observation volume obviously decreases as the flow rate is increased, as expected, the decay term due to fluorophore blinking remains remarkably constant. Accordingly, the measured fraction of protonated pyranine and the measured protonation relaxation time were not dependent on flow rate (Fig. 6b). Therefore, liquid flow does not influence the FCS measurement of the blinking parameters of pyranine.

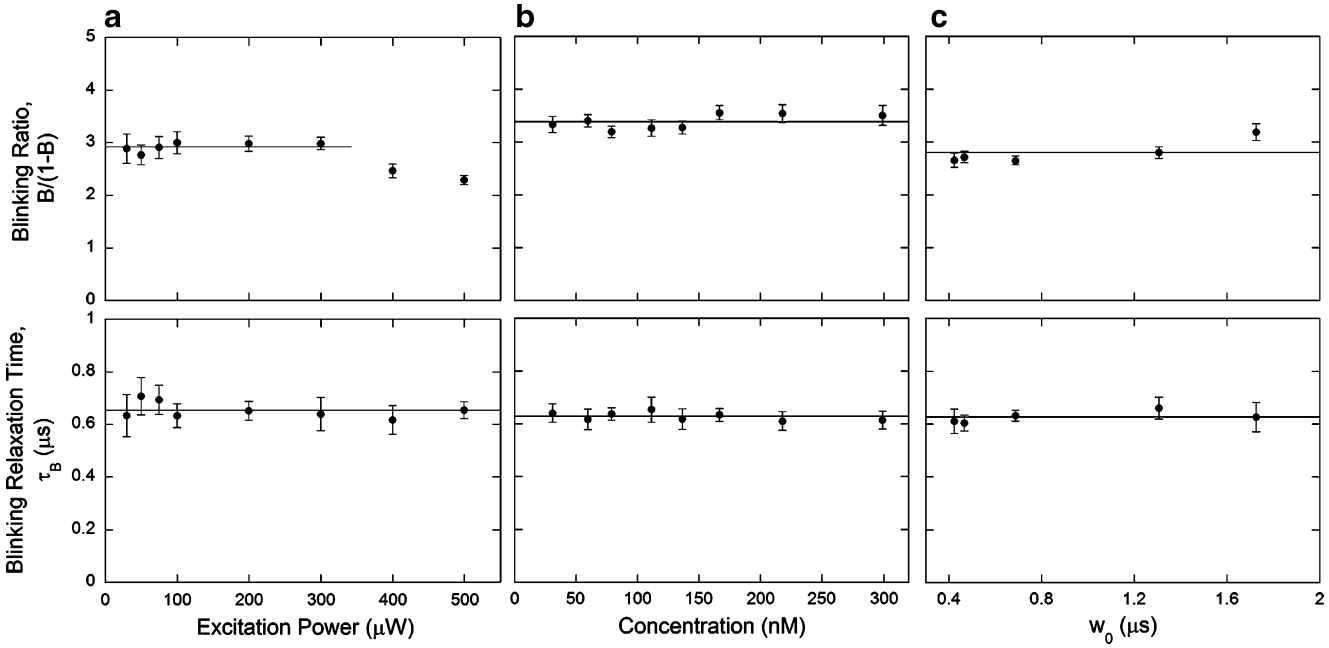

Fig. 5 Stability of pyranine photophysics parameters measured by FCS. Blinking ratio (*upper panels*) and blinking relaxation time (*lower panels*) against (**a**) the 442 nm excitation power, (**b**) the concentration of pyranine, and (**c**) the radius of the confocal detection volume. All pyranine samples were in PBS at pH=6.5 and at room temperature. Errors correspond to standard deviations

Influence of Buffer Composition and Solution Ionic Strength

One parameter known to influence protonation and deprotonation is the ionic environment of the molecule. The blinking of pyranine as detected by FCS will thus be dependent on buffer composition, and since this dependence cannot be avoided, it needs to be understood. Therefore, we next studied how different ions and their concentrations in the buffer influenced the protonation reaction. Starting from the PBS buffer used in all our previous experiments, we first investigated how varying the concentration of each individual buffer component affected the blinking of pyranine. The changes in the equilibrium constant and blinking relaxation time observed for these different components are shown in Fig. 7a, and the corresponding protonation and deprotonation rates are shown in Fig. 7b. Two important observations can be made. First, the protonation equilibrium constant is only weakly dependent on buffer composition (with *ln K* changing only by ~3% for increases in the ionic strength on the order of 70-fold), while the reaction relaxation time noticeably decreased with increasing buffer ionic strength as a result of an increase in both protonation and deprotonation rates. Second, the influence of the phosphate buffer (Na_2HPO_4 or KH_2PO_4) on the reaction rates (and

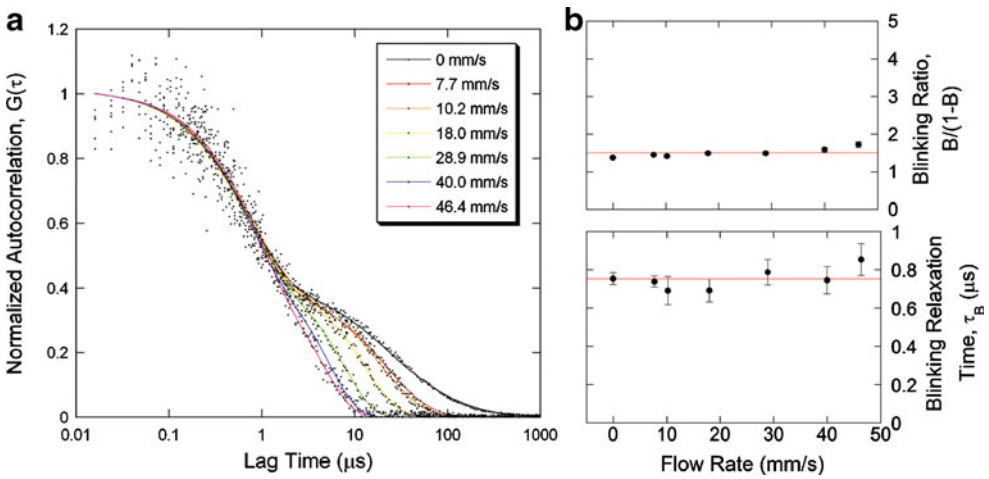

Fig. 6 Stability of pyranine photophysics parameters measurement by against flow rate. **a** Normalized autocorrelation function of pyranine obtained in a microfluidic channel at different flow rate. The ACFs were fitted with Eq. 2. **b** Blinking ratio (*upper panel*) and blinking relaxation time (*lower panel*) of pyranine obtained in microfluidic channel at various flow rates. Pyranine is in PBS at pH=7 and the measurements were taken at room temperature. Errors correspond to standard deviations

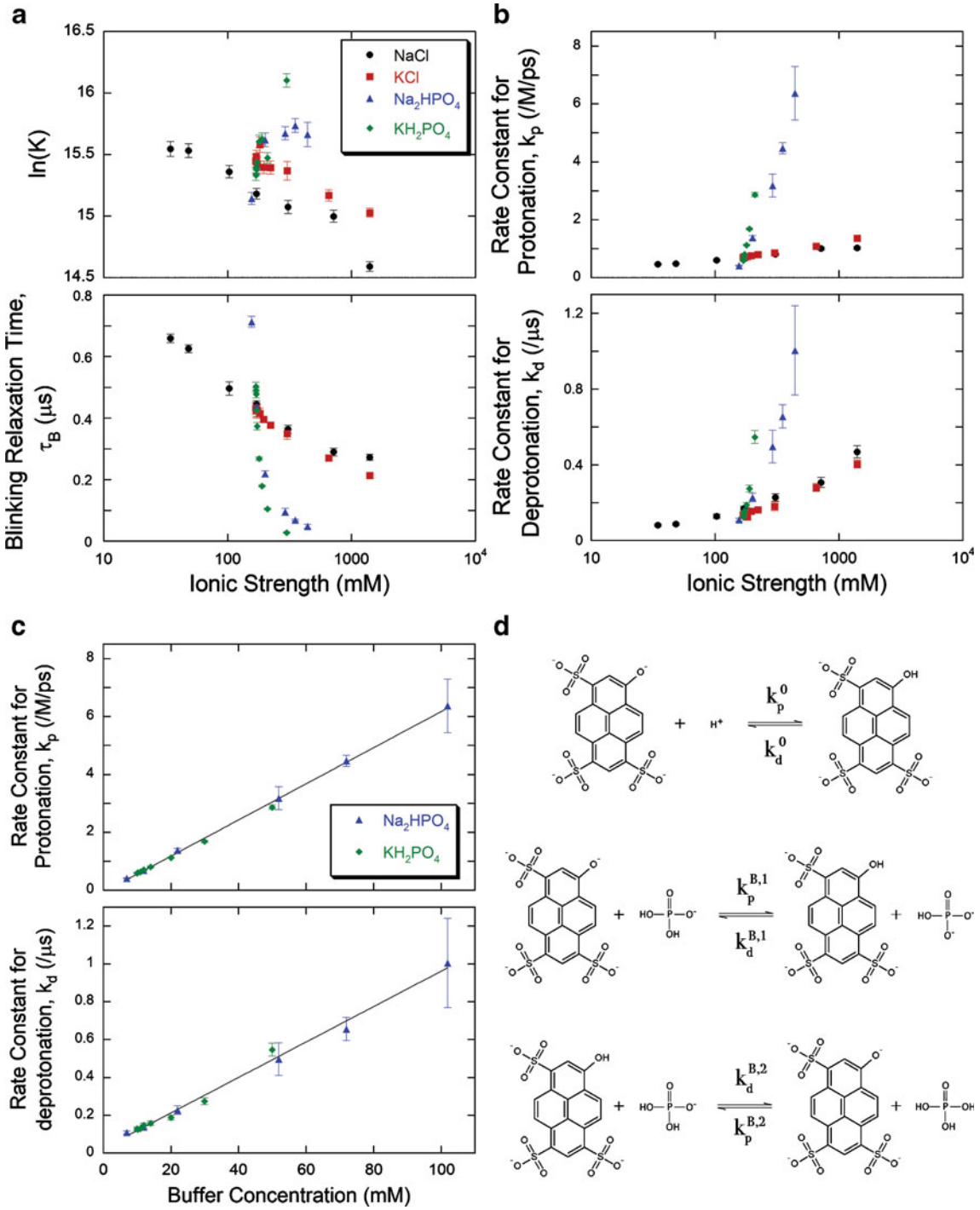

Fig. 7 Protonation / deprotonation dependence on buffer composition. **a** Equilibrium constant (*upper panels*) and relaxation time associated with the blinking (*lower panel*) as a function of ionic strength when varying buffer conditions. The buffer was PBS (pH= 5.5, room temperature) with the concentration of one component varied at a time. **b** Rate constant for protonation (*upper panel*) and rate constant for deprotonation (*lower panel*) as a function of ionic strength calculated from the data in (**a**). **c** Rate constant for protonation (*upper panel*) and rate constant for deprotonation (*lower panel*) as a function of buffer concentration. Data were fitted with Eq. 10. **d** Principal protonation and deprotonation pathways of pyranine in phosphate buffer at pH=5.5

therefore on relaxation time) is much stronger than that of the salts (NaCl and KCl). In the following, we therefore consider in turn the effect of buffers and the effect of salts.

It has been previously proposed that the presence of another molecule with acid-base properties (noted BH in its acidic form and B^- in its basic form in the following) could increase the probability of proton exchange for the

molecule of interest (in our case pyranine, noted AH in its acidic form and A^- in its basic form) due to direct interaction according to: $AH+B^- \leftrightarrows A^-+BH$ [20]. In this scenario, the rate for protonation (or deprotonation) of pyranine is therefore the sum of the reaction rate with an isolated proton ($AH \leftrightarrows A^-+H^+$), k_p^0 (or k_d^0), and of the reaction rate with the other acid-base molecule, k_p^B[Buffer] (or k_d^B[Buffer]). The rate constants for protonation and deprotonation as a function of buffer concentration (Na_2HPO_4 or KH_2PO_4, extracted from the data in Fig. 7b) are shown in Fig. 7c. They were fitted with the expression:

$$k_{p/d} = {k_{p/d}}^0 + {k_{p/d}}^B \cdot [Buffer] \quad (10)$$

The dependence on buffer concentration observed for the protonation and deprotonation rates of pyranine was indeed linear, therefore our data is consistent with the idea that phosphate molecules have a strong influence on the protonation of pyranine because direct proton exchange can occur between the two molecules. The parameters obtained from these fits are shown in Table 2. Given that the dihydrogen phosphate ion ($H_2PO_4^-$) is predominant form of phosphate at pH=5.5, the most likely pathways for protonation and deprotonation of pyranine at this pH are those represented in Fig. 7d. Considering that $[H_2PO_4^-] \approx$ [Buffer], the overall protonation and deprotonation rate constants due to the phosphate buffer can therefore be equated, at this pH, to: $k_p^B = 10^{pH} k_p^{B,1}$ and $k_d^B = k_d^{B,2}$, where $k_p^{B,1}$ and $k_d^{B,2}$ are the rate constant for pyranine protonation and deprotonation, respectively, due to direct interaction with a dihydrogen phosphate ion, as illustrated in Fig. 7d.

To better understand the effect of salts on pyranine protonation, we studied pyranine blinking in either phosphate buffer (10 mM Na_2HPO_4 and 2 mM KH_2PO_4, same as for PBS) or HEPES buffer (20 mM HEPES), at pH=5.5, and with varying concentrations of either monovalent (NaCl, KCl) or divalent ($MgCl_2$, $CaCl_2$) cations. The effect of these different salts on the equilibrium constant, relaxation time, protonation rate and deprotonation rate is shown in Fig. 8, where these parameters are plotted as a function of ionic strength. Strikingly, the values of K, τ_B, k_p and k_d measured for a given buffer and at a given ionic strength are almost the same for all the ions studied. This shows that, to a first approximation, the tested salts influence pyranine protonation only through the change in ionic strength they are causing.

Table 2 Values of k_p^0, k_d^0, k_p^B, and k_d^B obtained by analysis of the dependence of the protonation and deprotonation rates on phosphate buffer concentration (pH=5.5)

k_p^0 (/M/ps)	k_p^B (/M²/ps)	k_d^0 (/μs)	k_d^B (/M/μs)
0.01±0.01	57±1	0.040±0.007	8.5±0.5

The influence of ionic strength on the equilibrium of acid-base reactions has been studied by Boens *et al.* in the context the reversible protonation of BCECF [39]. They explained this influence in terms of the respective activities of the protonated and deprotonated form of the acid-base molecule, which depend on the ionic strength of the solution, μ, according to the Truesdell-Jones equation, an extended version of the Debye-Hückel equation. Taking into account these ionic-strength dependent activities allows rewriting the equilibrium constant for a reversible protonation reaction as [39]:

$$\log(K) = pK_a{}^0 - \left[A\left(z_2{}^2 - z_1{}^2\right)\frac{\sqrt{\mu}}{1+\dot{a}B\sqrt{\mu}} + L\mu\right] - \log(a_{H_2O}). \quad (11)$$

pK_a^0 is the value of the pK_a in the limit of low ionic strength. A and B are constants equal to A=0.51 and B=0.33 at room temperature and atmospheric pressure. z_1 and z_2 are the ionic charge of the protonated and deprotonated form of the acid-base molecule. $\dot{a}$ is the ionic radius of the molecule in angstroms. L is an adjustable parameter, which depends on the solution. a_{H_2O} is the water activity. In the case of pyranine ($z_1=-3$ and $z_2=-4$), Eq. 11 predicts that *log K* should decrease with increasing ionic strength, which is indeed what we observed for all the salts we studied (Fig. 8a and e). We fit our data with Eq. 11, fixing the water activity to 1, since it is ~1 in PBS [40]. The resulting values of pK_a^0, $\dot{a}$, and L obtained are listed in Table 3.

In contrast with what was observed for the equilibrium constant, the relaxation time associated with the protonation of pyranine had a very different dependence on ionic strength depending on the buffer. Whereas the relaxation time strongly decreases with ionic strength in phosphate buffer (Fig. 8b), it strongly increases with ionic strength in HEPES buffer (Fig. 8f). By looking at the rate constants, one can see that this difference stems from the dependence of the protonation rate on ionic strength. At pH=5.5, the protonation rate dominates the relaxation time, $\tau_B \sim (k_p[H^+])^{-1}$. And whereas k_p increases with ionic strength in phosphate buffer (Fig. 8c), it decreases with ionic strength in HEPES buffer (Fig. 8g). These opposite trends can be explained by taking into account the fact that, as discussed above, pyranine protonation (and deprotonation) is mostly due to direct interactions with buffer molecules, and that pyranine is a globally negatively charged molecule. At pH=5.5, the dominant form of phosphate is the negatively charged $H_2PO_4^-$, with lesser amounts of HPO_4^{2-}, whereas the dominant form of HEPES is the zwitterion $C_8H_{17}N_2O_3S$–OH, with lesser amounts of $C_8H_{18}N_2O_3S$–OH^+ and $C_8H_{17}N_2O_3S$-O^-. Increasing the ionic strength should result in an increase in the reaction rate between two negatively charged molecules, such as

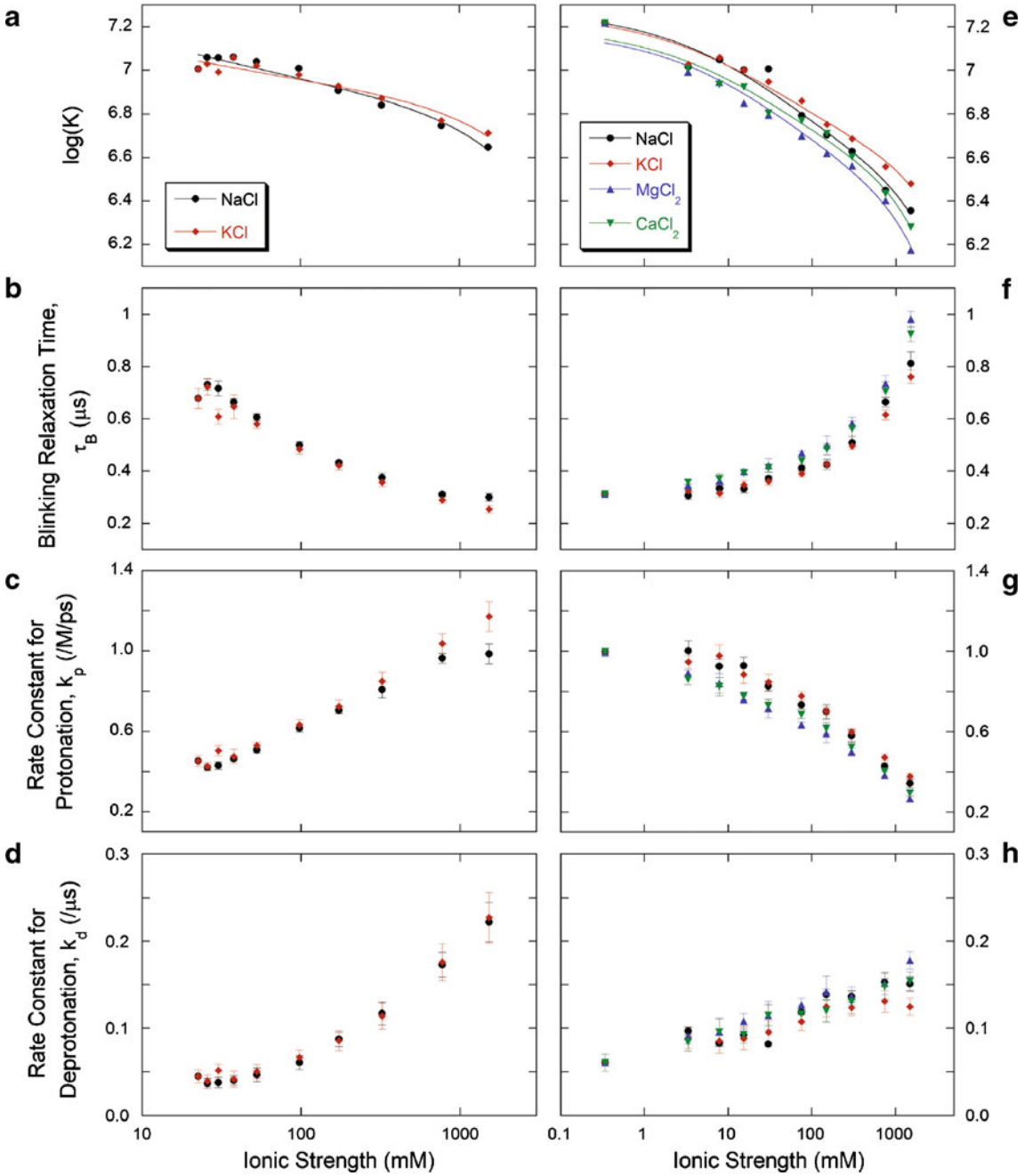

Fig. 8 Protonation / deprotonation dependence on ionic strength. Equilibrium constant (**a**, **e**) and blinking relaxation time (**b**, **f**) of pyranine as a function of ionic strength. Rate constant for protonation (**c**, **g**) and for deprotonation (**d**, **h**) of pyranine calculated from the data in (**a**, **b**, **e**, **f**). The buffer was 10 mM sodium phosphate and 2 mM potassium phosphate in (**a**–**d**), and 20 mM HEPES in (**e**–**h**). The legend indicates which salt was added in order to vary the ionic strength. All samples were at pH=5.5 and 20 °C. Lines in (**a**, **e**) are fit of the data with Eq. 11

pyranine and phosphate ions. Accordingly, the rates of phosphate buffer mediated protonation and deprotonation of pyranine increase with increasing solution ionic strength. Similarly, the rate of HEPES mediated deprotonation of pyranine increases with ionic strength, since the basic form of HEPES is also negatively charged. On the other hand, the acidic form of HEPES is a zwitterion, and as our results show, increasing the ionic strength decreases the protonation rate of pyranine, which could be because the rate of reaction between pyranine and HEPES decrease.

Table 3 Values of pK_a^0, $\dot{a}$, and L obtained from the analysis of the ionic-strength dependence of the equilibrium constant of the reversible protonation of pyranine (pH=5.5)

Buffer	pK_a^0	$\dot{a}$ [Å]	L
Phosphate buffer+NaCl	7.35±0.04	19±4	0.14±0.05
Phosphate buffer+KCl	7.28±0.04	24±6	0.12±0.04
HEPES buffer+NaCl	7.28±0.03	12±2	0.14±0.07
HEPES buffer+KCl	7.26±0.02	15±2	0.10±0.04
HEPES buffer+$MgCl_2$	7.19±0.03	13±2	0.18±0.06
HEPES buffer+$CaCl_2$	7.20±0.02	14±2	0.18±0.05

Discussion

Several observations support the idea that the fast ~1 μs decay of the autocorrelation functions obtained from pyranine solutions are due to fluorescence fluctuations caused by the reversible protonation of the molecule. First, we excited pyranine at a wavelength (442 nm) at which only the basic non-protonated form of the molecule is fluorescent, which means reversible protonation should result in fluorescence fluctuations. Second, the fluorescence fluctuations observed on the ~1 μs timescale do not depend on focal volume size, showing that they are not due to center of mass motions, nor do they depend on excitation intensity, showing that they are not due to intensity-dependent photophysical properties of pyranine, such as triplet transitions. Third, the observed fraction of non-fluorescent pyranine molecules decreases with increasing pH, according to the Henderson-Hasselbalch equation for the acid form of pyranine.

Our work suggests that pyranine can be used as a molecular thermometer, exactly as EGFP [22]. There are, however, a few important differences between the two molecules. First, pyranine is a small organic fluorophore, which can be more easily synthesized, stored and manipulated than the EGFP protein, and which therefore is more convenient for in vitro experiments. Second, whereas our previous study of EGFP photophysics showed that EGFP blinking could be detected reliably by FCS only for pH less than 6 (with very large measurement errors above that), the blinking of pyranine could be detected until pH=7 (with measurements errors, however, that also increased with pH). The reason behind this difference is that pyranine has a higher pK_a (7.2 at 20 °C) than EGFP. And whereas the strong temperature dependence observed for EGFP blinking relaxation time at low pH was lost when approaching physiological pH, the blinking relaxation time of pyranine retained a significant temperature dependence over the whole pH range studied, that is until pH=7. Thus pyranine, contrarily to EGFP, can be used as a molecular thermometer close to physiological pH. Third, the relaxation time associated with pyranine protonation is much faster (~1 μs or less) than that associated with EGFP protonation (~100 μs or more) in similar pH, temperature and buffer conditions. This is probably due to the fact that the hydroxyl group of pyranine is readily accessible, whereas that of EGFP is buried inside the barrel structure of the protein [20]. This is an advantage for FCS experiments, because it means the protonation term is better separated from the diffusion term in the autocorrelation functions measured by FCS (by 3 orders of magnitude for pyranine, and only ~1 order of magnitude for EGFP), thus the parameters associated with the protonation can be measured with a greater accuracy for pyranine. It also means pyranine can still be used as a temperature indicator under flow conditions. On the other hand, the maximum dynamic range exhibited by the relaxation time of pyranine protonation (a ~3-fold decrease in the range 15 °C to 55 °C at pH=7) is smaller than that exhibited by EGFP (~ 10-fold at pH=5), which means temperature measurements using pyranine can never achieve the same level of precision as those using EGFP under ideal conditions.

A major limitation of the temperature measurements we proposed previously, based on the measurement of fluorophore protonation relaxation time, τ_B, is that they need to be performed at fixed and known pH [22]. Similarly a major limitation of ratiometric pH measurements, based on the measurement of the ratio between protonated and deprotonated fluorophore, or B, is that they need to be performed at fixed and known temperature. Here, we have shown that using FCS to measure both τ_B and B, we can measure both temperature and pH in a single measurement. Our results show that the best working pH range is between 5 and 7 for pyranine, based on a comparison between measurements and theoretical predictions in Fig. 4c. In this region, the combined pH and temperature measurement gives us an uncertainty not exceeding ±0.2 for pH measurements. This uncertainty decreases for pH between 5.5 and 6.5, to ±0.1. The temperature measurement is less precise, with an uncertainty of ±5 °C.

The detection of the blinking of pyranine is a very robust measurement, which does not depend on fluorophore concentration, excitation intensity, fluorescence collection and detection efficiency, size of the confocal volume or liquid flow. However, it is very sensitive to buffer concentration. This issue has already been raised by Widengren and colleagues, who studied the effect of buffer concentration on pH measurements based on the detection of fluorophore blinking by FCS [20]. They showed that the total rate of the protonation/deprotonation reaction, which is the inverse of the blinking relaxation time, increases linearly with buffer concentration for fluorescein isothiocyanate, due to direct proton exchange between the buffer

molecules and the fluorophores. Our results suggests that direct proton exchange with phosphate ions also occurs for pyranine, and that it is a major contributor to the protonation of this molecule, where for example the deprotonation rate increases about 2-fold upon addition of 20 mM phosphate buffer at pH=5.5. Therefore the sensitivity of fluorophore blinking on buffer concentration seems inevitable, unless direct proton exchange with buffer molecules can be prevented. This means, however, that if temperature is precisely known, the value of the relaxation rate can be used to measure the concentration of a known buffer very accurately.

Pyranine blinking is also somewhat dependent on salt concentration. We found that the values of log(K) slightly decreased with increasing ionic strength of the solution. The influence of salts can be understood qualitatively in terms of the relative stability of the different forms of the molecule. Deprotonated pyranine is a tetra-anion, whereas protonated pyranine is a tri-anion. Therefore increasing the solution ionic strength, and therefore the effects of charge screening, will increase the stability of the deprotonated form of pyranine compared to its protonated form, thus decreasing K (Eq. 3). Since only the stability of the final products of the protonation/deprotonation reaction are important in this case, this result does not depend on the mechanism of protonation/deprotonation. Quantitatively, this effect is captured in the Truesdell-Jones equation, and its corollary, Eq. 11. Analysis of our data with these equations gave us good fits, and returned an average value for the ionic radius of pyranine (~16Å). This value is comparable to the ionic radius of other organic fluorophores, for example to the ionic radius of BCECF (~ 8Å) [39], and to those of other simple ions, for example the hydroxide ion (10.65Å) [41]. It is somewhat higher than the value of the hydrodynamic radius of the molecule that can be calculated from our FCS data (~6Å). For the other adjustable parameter in the fit, L, we also found values in the same range as those found for other ions in ref [41].

The picture gets more complicated however when considering separately the dependence of the protonation and deprotonation rates on ionic strength. Whereas the deprotonation rate increases with increasing ionic strength both in phosphate and HEPES buffers, the protonation rate dependence on ionic strength is very different in both buffers. The protonation rate increases with ionic strength in phosphate buffers, but decreases with ionic strength in HEPES buffer. This can be explained qualitatively by remembering that protonation occurs in large part through direct interactions between buffer and pyranine molecules, and by considering that phosphate and HEPES buffers have very different charges (phosphate ions are negatively charged, HEPES is a zwitterion). Therefore charge screening through increase of the solution ionic strength is indeed expected to increase direct interactions between the negatively charged pyranine and the negatively charged phosphate ions, and therefore buffer-mediated protonation. It may have an opposite effect in the case of HEPES, a zwitterion. In support of the theory that protonation/deprotonation rates depends on ionic strength mainly because of interactions between the fluorophore and the buffer molecules, Widengren et al. found that NaCl alone in the solution would not change the rate of the proton exchange [20], while we observed that varying the concentration of chloride salts in buffer influences the reversible protonation rate.

In conclusion, we note that the method we propose to measure both pH and temperature in a single FCS measurement should be useful for measurements in biological sample because heat production and proton transfer are coupled reactions in many cellular processes. However, one must keep in mind that the protonation kinetics of pyranine is very dependent on buffer and salt concentration, and that this dependence is complex. Since buffer and ionic concentrations are not well characterized in all cell types, this remains at present the major limitation of this method for cellular applications. However, we note that the equilibrium constant associated with the protonation reaction (or, equivalently, B), depends only slightly on ionic concentration at least at low buffer concentrations. Therefore pH measurements based on ratiometric methods (i.e. on the measurement of B) will still be reasonably accurate.

References

1. Li Jeon N, Baskaran H, Dertinger SK, Whitesides GM, Van de Water L, Toner M (2002) Neutrophil chemotaxis in linear and complex gradients of interleukin-8 formed in a microfabricated device. Nat Biotechnol 20(8):826–830
2. Jeon SM, Turner J, Granick S (2003) Noncontact temperature measurement in microliter-sized volumes using fluorescent-labeled DNA oligomers. J Am Chem Soc 125(33):9908–9909
3. Ross D, Gaitan M, Locascio LE (2001) Temperature measurement in microfluidic systems using a temperature-dependent fluorescent dye. Anal Chem 73(17):4117–4123
4. Erickson D, Sinton D, Li DQ (2003) Joule heating and heat transfer in poly(dimethylsiloxane) microfluidic systems. Lab Chip 3(3):141–149
5. Clapham DE (2007) Calcium signaling. Cell 131(6):1047–1058
6. Kholodenko BN (2009) Spatially distributed cell signalling. FEBS Lett 583(24):4006–4012
7. Lowell BB, Spiegelman BM (2000) Towards a molecular understanding of adaptive thermogenesis. Nature 404(6778):652–660
8. Straubinger RM, Papahadjopoulos D, Hong K (1990) Endocytosis and intracellular fate of liposomes using pyranine as a probe. Biochem 29(20):4929–4939
9. Overly CC, Lee KD, Berthiaume E, Hollenbeck PJ (1995) Quantitative measurement of intraorganelle pH in the endosomal lysosomal pathway in neurons by using ratiometric imaging with pyranine. PNAS USA 92(8):3156–3160

10. Krueger KM, Daaka Y, Pitcher JA, Lefkowitz RJ (1997) The role of sequestration in G protein-coupled receptor resensitization—Regulation of beta(2)-adrenergic receptor dephosphorylation by vesicular acidification. J Biol Chem 272(1):5–8
11. Nakamura T, Matsuoka I (1978) Calorimetric studies of heat of respiration of mitochondria. J Biochem 84(1):39–46
12. Suzuki M, Tseeb V, Oyama K, Ishiwata S (2007) Microscopic detection of thermogenesis in a single HeLa cell. Biophys J 92(6): L46–48
13. Rink TJ, Tsien RY, Pozzan T (1982) Cytoplasmic Ph and free Mg-2+ in lymphocytes. J Cell Biol 95(1):189–196
14. Kato H, Nishizaka T, Iga T, Kinosita K, Ishiwata S (1999) Imaging of thermal activation of actomyosin motors. PNAS USA 96(17):9602–9606
15. Grynkiewicz G, Poenie M, Tsien RY (1985) A new generation of Ca2+ indicators with greatly improved fluorescence properties. J Biol Chem 260(6):3440–3450
16. Willoughby D, Thomas RC, Schwiening CJ (1998) Comparison of simultaneous pH measurements made with 8-hydroxypyrene-1, 3, 6-trisulphonic acid (HPTS) and pit-sensitive microelectrodes in snail neurones. Pflugers Archiv-Europ J Phys 436(4):615–622
17. Herman P, Drapalova H, Muzikova R, Vecer J (2005) Electroporative adjustment of pH in living yeast cells: ratiometric fluorescence pH imaging. J Fluoresc 15(5):763–768
18. Ito S, Sugiyama T, Toitani N, Katayama G, Miyasaka H (2007) Application of fluorescence correlation spectroscopy to the measurement of local temperature in solutions under optical trapping condition. J Phys Chem B 111(9):2365–2371
19. Sanders R, Draaijer A, Gerritsen HC, Houpt PM, Levine YK (1995) Quantitative pH imaging in cells using confocal fluorescence lifetime imaging microscopy. Anal Biochem 227(2):302–308
20. Widengren J, Terry B, Rigler R (1999) Protonation kinetics of GFP and FITC investigated by FCS—aspects of the use of fluorescent indicators for measuring pH. Chem Phys 249(2–3):259–271
21. Hess ST, Heikal AA, Webb WW (2004) Fluorescence photoconversion kinetics in novel green fluorescent protein pH sensors (pHluorins). J Phys Chem B 108(28):10138–10148
22. Wong FHC, Banks DS, Abu-Arish A, Fradin C (2007) A molecular thermometer based on fluorescent protein blinking. J Am Chem Soc 129(34):10302–10303
23. Haupts U, Maiti S, Schwille P, Webb WW (1998) Dynamics of fluorescence fluctuations in green fluorescent protein observed by fluorescence correlation spectroscopy. PNAS USA 95(23):13573–13578
24. Wolfbeis OS, Furlinger E, Kroneis H, Marsoner H (1983) Fluorimetric analysis. 1. A study on fluorescent indicators for measuring near neutral (Physiological) pH-values. Fres Zeit Anal Chem 314(2):119–124
25. Kano K, Fendler JH (1978) Pyranine as a sensitive Ph probe for liposome interiors and surfaces—pH gradients across phospholipid vesicles. Biochim Biophys Acta 509(2):289–299
26. Huppert D, Kolodney E, Gutman M, Nachliel E (1982) Effect of water activity on the rate of proton dissociation. J Am Chem Soc 104(25):6949–6953
27. Pines E, Huppert D, Agmon N (1991) Salt effects on steady-state quantum yields of ultrafast, diffusion-influenced, reversible photoacid dissociation reactions. J Phys Chem 95(2):666–674
28. Rini M, Magnes BZ, Pines E, Nibbering ETJ (2003) Real-time observation of bimodal proton transfer in acid-base pairs in water. Science 301(5631):349–352
29. Rini M, Pines D, Magnes BZ, Pines E, Nibbering ETJ (2004) Bimodal proton transfer in acid-base reactions in water. J Chem Phys 121(19):9593–9610
30. Mohammed OF, Pines D, Dreyer J, Pines E, Nibbering ETJ (2005) Sequential proton transfer through water bridges in acid-base reactions. Science 310(5745):83–86
31. Cox MJ, Bakker HJ (2008) Parallel proton transfer pathways in aqueous acid-base reactions. J Chem Phys 128(17):174501
32. Cox MJ, Siwick BJ, Bakker HJ (2009) Influence of ions on aqueous acid-base reactions. Chemphyschem 10(1):236–244
33. Stellwagen E, Prantner JD, Stellwagen NC (2008) Do zwitterions contribute to the ionic strength of a solution? Anal Biochem 373 (2):407–409
34. Banks DS, Fradin C (2005) Anomalous diffusion of proteins due to molecular crowding. Biophys J 89(5):2960–2971
35. Petrasek Z, Schwille P (2008) Precise measurement of diffusion coefficients using scanning fluorescence correlation spectroscopy. Biophys J 94(4):1437–1448
36. Magde D, Webb WW, Elson EL (1978) Fluorescence correlation spectroscopy. 3. Uniform translation and laminar-flow. Biopolymers 17(2):361–376
37. Satsoura D, Leber B, Andrews DW, Fradin C (2007) Circumvention of fluorophore photobleaching in fluorescence fluctuation experiments: a beam scanning approach. Chemphyschem 8(6):834–848
38. Avnir Y, Barenholz Y (2005) pH determination by pyranine: medium-related artifacts and their correction. Anal Biochem 347 (1):34–41
39. Boens N, Qin WW, Basaric N, Orte A, Talavera EM, Alvarez-Pez JM (2006) Photophysics of the fluorescent pH indicator BCECF. J Phys Chem A 110(30):9334–9343
40. Ross A, Kearney JN (2004) The measurement of water activity in allogeneic skin grafts preserved using high concentration glycerol or propylene glycol. Cell Tissue Banking 5(1):37–44
41. Langmuir D (1997) Aqueous environmental geochemistry. Prentice-Hall, Upper Saddle River